# Using Proper Orthogonal Decomposition Methods for Comparing CFD Results to Experimental Measurements

T. Andrianne
A. Guissart
V. Terrapon
G. Dimitriadis

University of Liège
Liège, 4000
Belgium
t.andrianne@ulg.ac.be

## Abstract

This work presents a method for quantitative comparison of numerical results to experimental measurements. It is based on the concept of Proper Orthogonal Decomposition. This technique is selected in order to compare the unsteady aerodynamic flows around static and oscillating bodies obtained from wind tunnel testing and numerical simulations. Two dimensional Time-resolved Particle Image Velocimetry measurements are carried-out on the upper surface a 4:1 rectangular cylinder. Simulations are performed using unsteady Reynolds-Averaged Navier-Stokes and an unsteady Discrete Vortex Method. It is demonstrated that the proposed technique is a good preliminary step for comparing the main characteristics of unsteady aerodynamic data.

Key words: unsteady aerodynamics, proper orthogonal decomposition, particle image velocimetry, CFD

## Introduction

Over the last decades, our understanding of complex aerodynamic flows has been strongly intensified. The effect of small turbulent structures in unsteady flow-fields can now be taken into account in large computational models [1]. On the other hand, experimental analysis also became more advanced, especially with the Time-resolved Particle Image Velocimetry (Tr-PIV) technique [2], which allows the measurement of highly unsteady phenomena occurring at small and large scales in the flow-field around a body [3], [4]. In parallel to these exciting evolutions, the need for reliable comparison techniques of the resulting numerical and experimental data is also becoming more important.

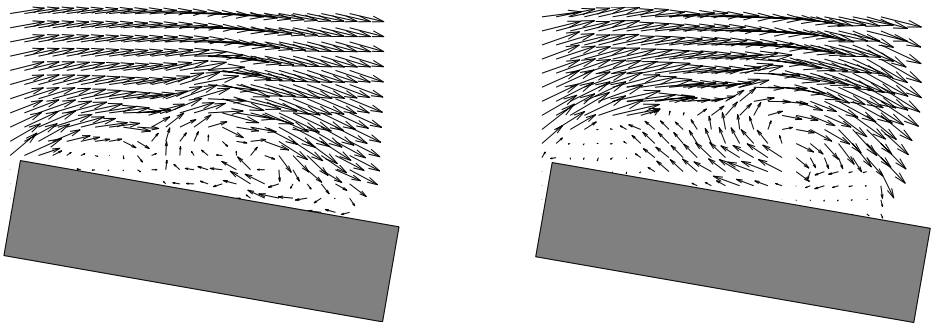

**Figure 1: Snapshots of the velocity fields over an oscillating 4:1 rectangular cylinder Experiments (left), Simulations (right)**

Figure 1 shows two instantaneous snapshots of the velocity fields on the upper surface of a rectangle which undergoes pitching oscillations around its geometric center. The snapshots are measured and simulated when the rectangle reaches the maximum pitch angle of the upstroke motion. Despite the relative resemblance of these two snapshots, it is not practical to repeat this comparison for all the simulation and experimental observations (300 snapshots in this case). Furthermore, because of the measurement noise present in the Tr-PIV data, it is vain to try to compare the absolute value of the velocity components at all the location of the grid points of the observation window.

It is proposed to use the Proper Orthogonal Decomposition (POD) technique in order to extract the main characteristics of the simulated and measured velocity fields and to facilitate the comparison.

This paper first presents the basic properties of the POD technique when applied on unsteady velocity fields u(x,y,t) and v(x,y,t). The use of the Modal Assurance Criterion (MAC) is also introduced in this section. Then the approach is applied to two applications, dealing with a 2D bluff body in a subsonic flow-field. In particular, a rectangular cylinder characterized by an aspect ratio *c/d* equal to 4 is chosen. This specific aspect ratio leads to interesting flow separation and re-attachment on its surface. Hence, it constitutes a good test case for the validation of the proposed comparison technique.

The two applications concern the analysis of the unsteady flow-field on the upper surface of the rectangle when it is:

1. statically set at an angle of attack equal to 5°,
2. oscillating in pitch around its mid-chord point at an imposed frequency and amplitude.

For each application, Tr-PIV measurements and numerical simulations, using Discrete Vortex Method (DVM), are performed. In the case of the static rectangle, Reynolds-Averaged Navier-Stokes (RANS) simulations are additionally carried out using OpenFOAM. The main characteristics of both numerical models are described and results about for quantities such as aerodynamic force coefficients and Strouhal number are presented. Finally, we focus on the comparison between numerical and experimental unsteady flow velocities using the POD technique.

## Proper Orthogonal Decomposition

The POD approach consists in calculating a set of proper orthogonal functions in order to decompose the signal with the objective to capture the maximum amount of energy. The 2D unsteady flow-fields u(x,y,t) and v(x,y,t) can be expressed as

$$u(x,y,t) = \sum_{i=1}^{M} q_i(t)\, \Phi_{u,i}(x,y) \qquad \text{and} \qquad v(x,y,t) = \sum_{i=1}^{M} q_i(t)\, \Phi_{v,i}(x,y)$$

where M denotes the number of time instances. $\Phi_{u,i}(x,y)$ and $\Phi_{v,i}(x,y)$ are the POD modes, which only depend on the spatial coordinates (x,y). The generalized coordinates $q_i(t)$ represent the time dependence of the velocity field. The main advantage of POD is that no a priori knowledge about the data is needed. More details on the implementation of the POD technique can be found in reference [5].

The objective of the method is to apply the POD technique to the numerical results and experimental measurements, and to compare its outputs. In this paper, the quantitative comparison of the spatial patterns, the POD modes, is carried on using the Modal Assurance Criterion (MAC) [6]. The concept of MAC is commonly used in the field of structural dynamics in order to compare the mode shapes obtained from experimental modal analysis to the ones computed from finite elements models [7].

The value of the MAC is defined for each experimental (EXP) and numerical (NUM) couple of POD modes $(\Phi_i^{EXP}, \Phi_j^{NUM})$ by

$$MAC(\Phi_i^{EXP}, \Phi_j^{NUM}) = \left( \frac{\Phi_i^{EXP} . \Phi_j^{NUM}}{\|\Phi_i^{EXP}\| \|\Phi_j^{NUM}\|} \right)^2$$

The value of $MAC(\Phi_i^{EXP}, \Phi_j^{NUM})$ varies between 1 and 0, depending if the i$^{th}$ experimental POD mode $\Phi_i^{EXP}$ is equivalent, or not, to the j$^{th}$ numerical POD mode $\Phi_j^{NUM}$.

## Unsteady flow around a static body

The first application concerns the modelisation of the unsteady flow around the rectangle at an angle of attack of 5°. The Reynolds number, based on the chord of the rectangle is equal to $Re = 10^5$.

As stated in the introduction, two numerical tools are used for simulating the flow around the rectangle. They are presented concisely below.

### DVM model

The DVM model is based on the Lagrangian approach, which consists in shedding vortex particles on the surface of the rectangle and to track them individually at each time step [8]. Several studies have demonstrated that the DVM technique is well suited for simulating the unsteady flow-field around bluff structures (see for example [9] or [10]). This is due to the large separation and re-attachment of the flow-field around the sharp edges of the bluff body. Furthermore, the DVM tool is very interesting in terms of numerical cost, because it adds vortex particles where more details are required, i.e. in the vicinity of the upper surface of the body. The regions of the fluid domain not affect by the presence of the body are not taken into account (no vortex particles). This natural refinement of DVM avoids over-refined zones such as the boundary layer around the body that are necessary in CFD based methods.

The number of panels discretizing the geometry of the rectangle is set to 350. The time step is chosen as $dt = 0.1\, c / V_\infty$, where $c$ is the chord of the rectangle and $V_\infty$ is the free-stream velocity of the incoming flow-field. The detailed description of the implementation can be found in Ref. [9].

### Unsteady Reynolds-Averaged Navier-Stokes (RANS) simulations

Two-dimensional unsteady RANS simulations are also performed one the same case using the open source CFD code OpenFOAM[1], which is based on the finite volume method for unstructured meshes. For the purpose of this study, the transient solver for incompressible flows pisoFoam based on the PISO algorithm [11] is used.

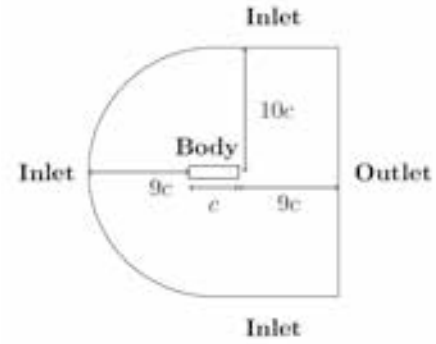


**Figure 2: Computational domain for the RANS simulations**

[1] www.openfoam.com
[2] http://geuz.org/gmsh/

The dimensions corresponding to computational domain are represented in Figure 2. The hexahedral mesh, created with GMSH[2], is divided into two regions as shown in Figure 3. In order to have an adequate resolution and accuracy in the critical flow regions, in particular where flow separation is expected, a fine structured mesh is used in the vicinity of the rectangle and in its wake (see the detailed view in Figure 3).

Because no wall-function is used, the first mesh point away from the rectangle surface is set such that $y^+ \approx 1$, where the + exponent indicates wall units, for most of the cells around the rectangle. A grid convergence analysis on four different meshes (i.e., with around 310 000 , 140 000, 80 000 and 36 000 cells, respectively) has shown that the solution is grid-independent. The following results were obtained on the 140 000 cells mesh, the computation on the finest one being too slow.

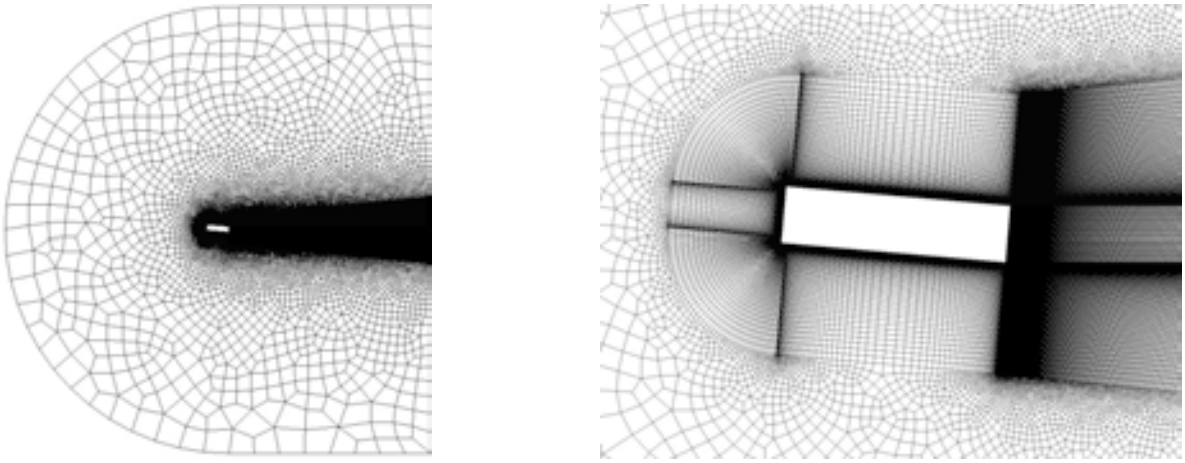

**Figure 3: Computational mesh for the RANS simulations: entire computational domain (left) and detailed view of the regions close to the rectangle (right)**

To close the RANS equations, the Menter k-ω SST model [11] is employed, as it is known to be better to predict flow separations than the standard k-ε model and to be less sensitive to free-stream turbulence than the standard k-ω model [13].

The backward Euler scheme is used to advance the equations in time. In order to capture accurately the smallest time scales of the flow and to ensure numerical stability, the time step is chose to be $10^{-4}$. This corresponds to a CFL of about 0.9 and 18 000 times steps per shedding period.

At the boundary surface, the no-slip condition is imposed for the velocity, a homogeneous Neumann condition for pressure, and Dirichlet conditions for the turbulent scalars. At the inlet, the free-stream velocity ant turbulent scalars are imposed. The latters correspond to the wind-tunnel free-stream turbulence intensity of 0.15% [9].
For the pressure, a zero-gradient boundary condition is set. Finally, the outlet corresponds to a zero-gradient for the velocity and turbulent scalars, while the pressure is enforced.

## Preliminary analysis

On the basis of the two numerical tools presented above, the following global quantities are computed: the mean aerodynamic force coefficients $C_L$, $C_D$ and the Strouhal number, defined by $St = f\, d / V_\infty$, where $f$ is the shedding frequency and $d$ is the thickness of the rectangle. These results are summarized in Table 1 for the two numerical simulations, together with experimental results from the literature [14] and previous works of the authors [9].

[2] http://geuz.org/gmsh/

**Table 1: Mean aerodynamic lift and drag coefficients and Strouhal number for the flow around a rectangle of aspect ratio of 4 at 5° angle of attack and Re=$10^5$.**

| | $C_L$ | $C_D$ | *St* |
|---|---|---|---|
| DVM | 0,56 | 0,32 | 0,143 |
| Unsteady RANS | 0,83 | 0,45 | 0,136 |
| Experiments | 0,53 | 0,45 | 0,152 |

It is observed from this table that the two numerical tools are not capable to predict accurately the values of $C_L$, $C_D$ and *St*. The lift coefficient and the Strouhal number are well estimated by the DVM code but the drag coefficient is too small in comparison with experiments. On the other hand, RANS accurately predict the drag coefficient but the lift coefficient is over-estimated. The error on the Strouhal number is acceptable. Note that eddy viscosity models are know to be inaccurate for separated flows.

Up to this point, the main characteristics of the two numerical tools have been presented, together with some basic global results. It is proposed to push further the understanding of the unsteady phenomena taking place around the rectangle by analyzing the flow-field on its upper surface.

## POD analysis

The unsteady flow-field is measured and computed on the upper surface of the cylinder, on a mesh of 25 by 13 points as shown by crosses in Figure 4. In this figure, the rectangle is shown in gray and the flow comes from the left of the image.

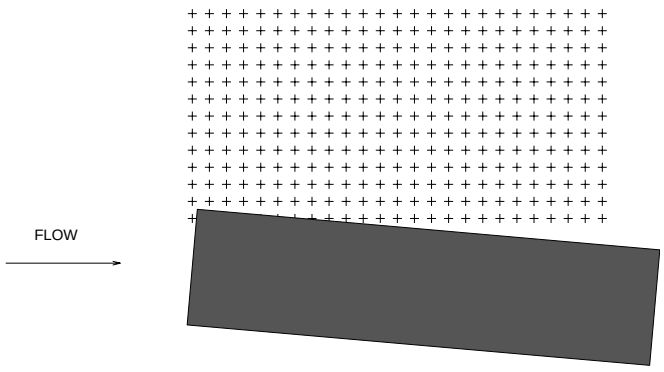


**Figure 4: Observation window on the upper surface of the static cylinder at 5°**

The POD technique is applied to the velocity fields obtained from the PIV measurements and the two numerical tools. We concentrate here on the comparison of the spatial patterns (POD modes) and their energy content. Figure 5 shows the six first modes obtained by decomposing the experimental and numerical results. It is based on 500 time instances and the sample length corresponds to 50 shedding periods.

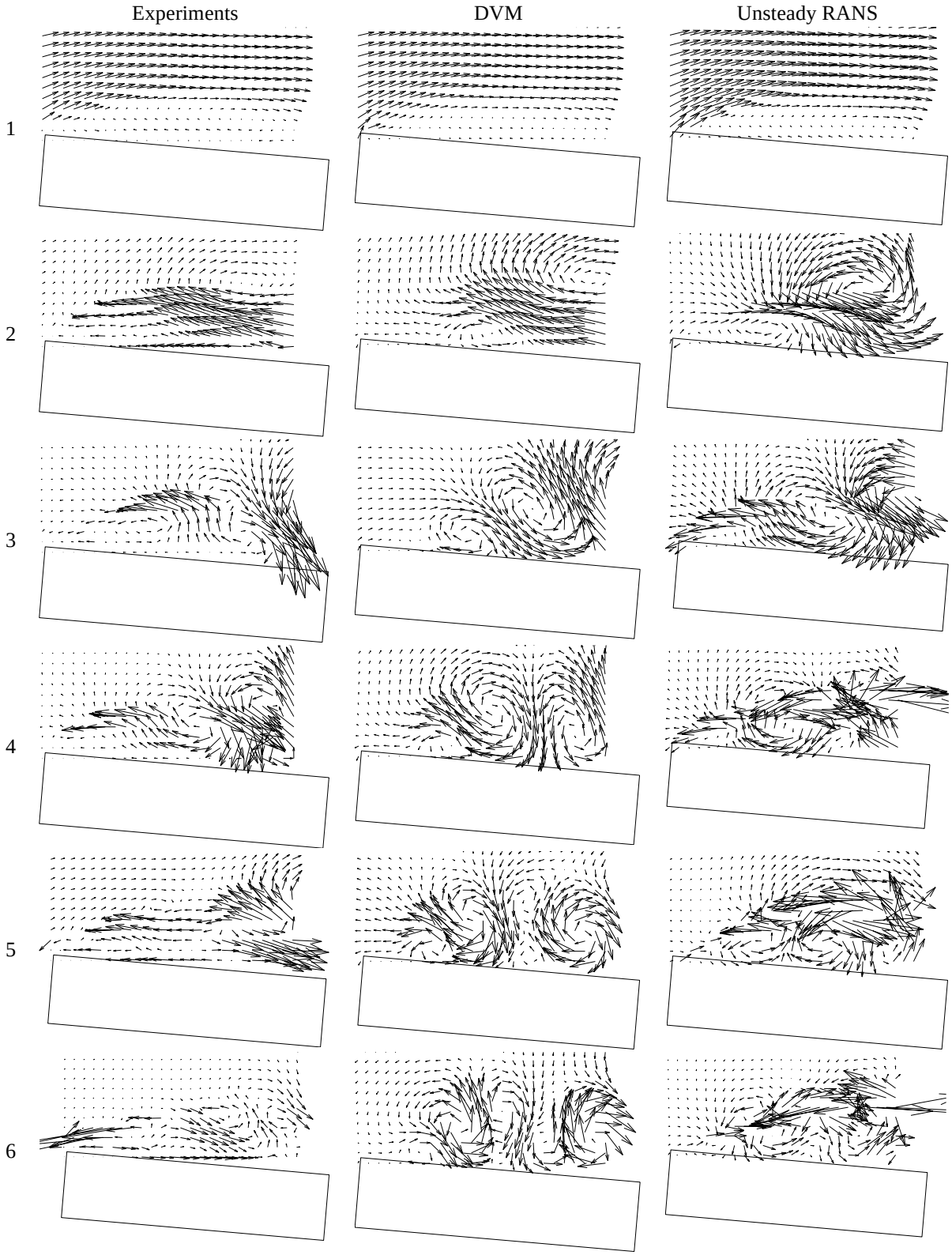


**Figure 5: First six POD modes: Experiments (left), DVM (center), Unsteady RANS (right)**

One can observe that the first POD mode is correctly capture by both numerical models. This mode corresponds to the mean flow, because the mean value of the fields u(x,y,t) and v(x,y,t) are not subtracted when applying the POD technique (see [5] for details about the consideration of the mean flow in the POD analysis). Nevertheless, the phenomena of interest are typically related to the unsteadiness of the flow-field. Hence, it is necessary to analyze the other POD modes. The second POD mode is relatively well captured by the DVM simulation. On the other hand, fewer similarities can be observed observed with the unsteady RANS. It is also very interesting to note that the third mode given by the unsteady RANS is very similar to the fourth experimental mode.

Generally speaking, it is difficult to have a global view of the resemblance of the numerical POD modes, with the experimental ones. Hence, it is proposed to use the MAC to obtain a more quantitative comparison between the three different sets of results. A 6 by 6 MAC matrix is calculated for each numerical results (DVM and Unsteady RANS), taking into account the first six modes presented in Figure 5. These two matrices are shown graphically in Figure 6.

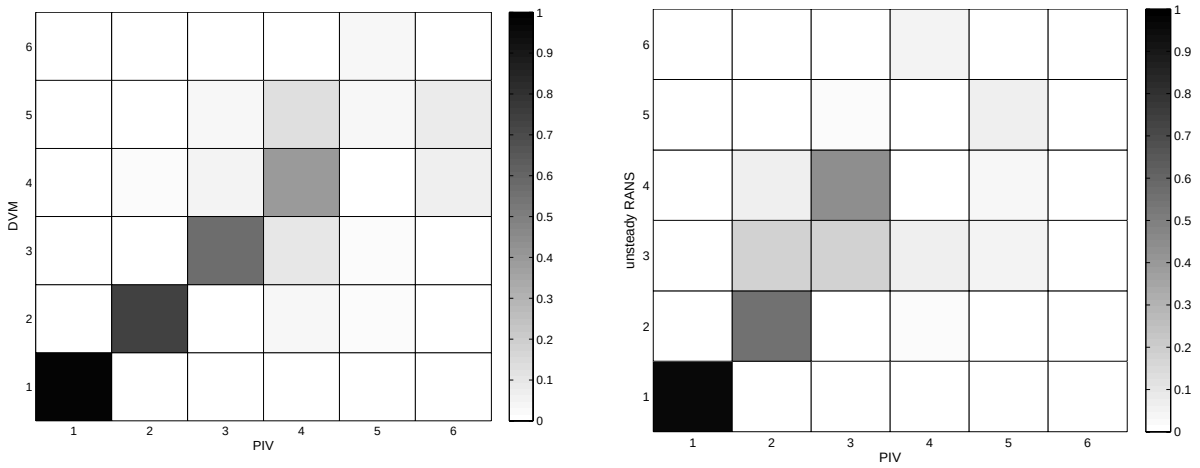


**Figure 6: Static rectangle at 5° - MAC matrices**
**DVM vs Experiments (left), Unsteady RANS vs Experiments (right)**

It is observed that the first four POD modes from the DVM simulations are well reproduced (MAC values higher than 0.4). On the other hand, only the first and second POD modes seem to be correctly captured by the unsteady RANS. As qualitatively observed from Figure 5, the MAC analysis confirms that the third POD mode from the unsteady RANS simulation corresponds to the fourth experimental mode (with a MAC value of 0.45 off the diagonal). Hence, three POD modes are relatively well identified using unsteady RANS simulations.

It is interesting to analyze the eigenvalues corresponding to each of the first six POD modes. These quantities are proportional to the kinetic energy of the POD modes [5]. They are plotted in Figure 7, where it is clear that the first POD mode ('mean flow' mode) contains most of the energy of the flow. For the experimental, the DVM and the unsteady RANS results, the energy content of this mode is equal to 97.6%, 95.9% and 99.4%, respectively.

An enlarged view on the eigenvalues 2 to 6 is shown in Figure 7. Despite their low absolute values, the energy content is distributed over these POD modes in the case of experiments and DVM results. In order to emphasis this observation, Figure 8 presents the residual energy percentage for modes 2 to 6. The residual energy is defined by the ratio of the eigenvalue of a mode divided by the sum of the eigenvalues for modes 2 to 6. From Figure 8, it is clear that each POD mode between 2 and 4 contains between 10% and 30% of the residual energy in the case of the experiments and the DVM simulations. On the other hand, the POD modes 2 and 3 from the unsteady RANS simulations contain most of the energy of the flow-field, the contribution of modes 4, 5 and 6 being negligible.

This discussion about the energy distribution is in agreement with the observations made about the MAC matrices in Figure 6. If a POD mode does not appear in a simulated set of data, its energy content is very low

and the corresponding element of the MAC matrix is also close to zero. Note that the information about the energy level of a POD mode can be used in the case of Reduce Order Modelling, where it can orient the choice of the retained modes for reconstructing the signal.

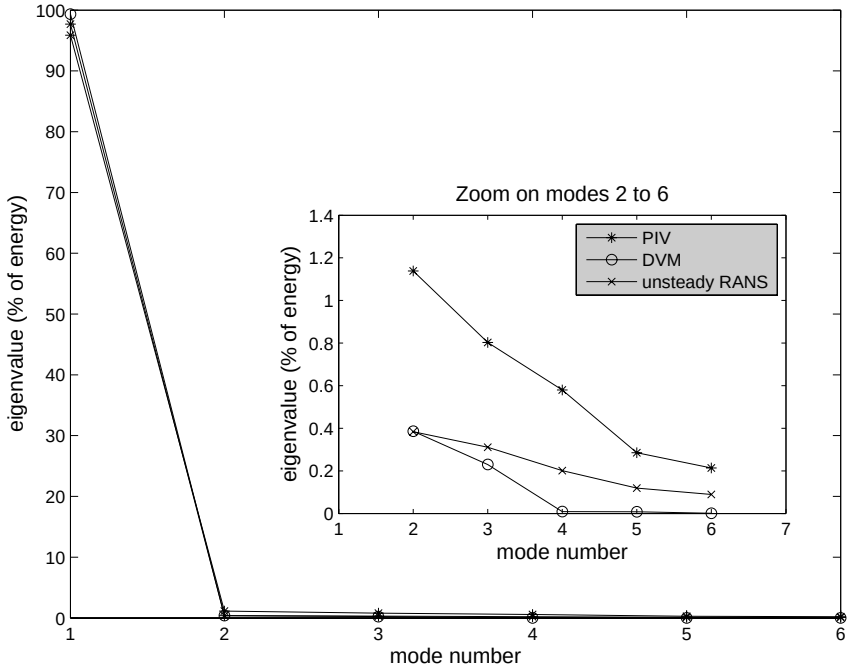


**Figure 7: Static rectangle at 5° - Eigenvalues of the POD modes: percentage of the total flow energy**

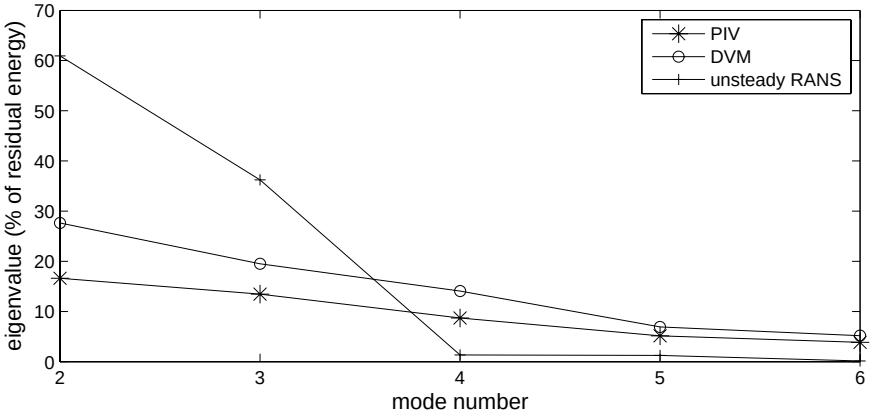


**Figure 8: Static rectangle at 5° - Eigenvalues of POD modes 2 to 6: percentage of the residual flow energy**

## Unsteady flow around an oscillating body

The second application of this paper concerns the analysis of the flow-field around the oscillating rectangle. A pitching motion is applied to the rectangle according to $\alpha(t)=10°\sin(2\pi 8.1t)$, where *t* is the dimensional time, expressed in seconds. The Reynolds number is identical to the one of the static case above.
This application involves only DVM simulations and its comparison with the Tr-PIV measurements is performed on the upper surface of the rectangle. The observation window is slightly bigger than for the static case, as shown in Figure 9. In this figure, the dashed rectangle represents the center of oscillation at 0°. The two plain rectangles correspond to the maximum and minimum values of the pitch angle (+/- 10°). Note that the position of the observation window enable to cover the entire upper surface of the rectangle when it reaches its maximum and minimum pitching positions.

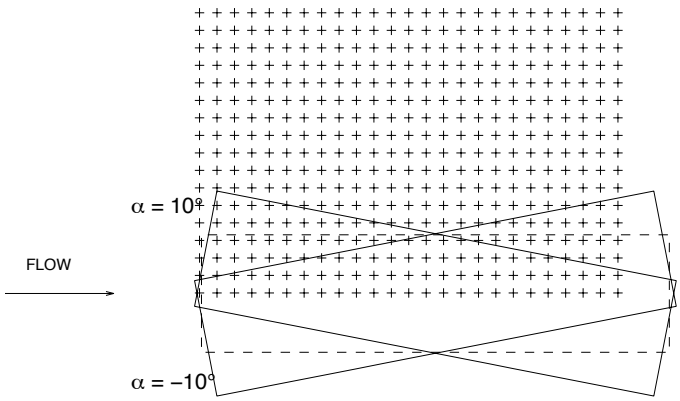


**Figure 9: Observation window on the upper surface of the cylinder for the oscillating cylinder**

The numerical parameters of the static application are retained in this section, hence no description of the DVM simulations is presented here.

Experimental measurements are performed during three periods of oscillation of the rectangle. A preliminary computation is carried out using the DVM tool in order to get rid of the starting effects. This fast initial step lasts 10 pitching oscillations. Then flow is computed in the observation window during three pitching oscillations and is saved for further post-processing.

### POD analysis

Similarly to the static rectangle case, the POD technique is applied on the computed unsteady velocity fields u(x,y,t) and v(x,y,t). Nevertheless, because of the oscillation of the rectangle in the observation window, some grid points will periodically be inside the solid domain, where the components of the velocity vanish. It is decided here to keep these zero values, i.e. $u(x_i,y_i,t_i) = v(x_i,y_i,t_i) = 0$, where $(x_i,y_i,t_i)$ denotes the coordinates of the grid points inside the rectangle.

The MAC matrix built from the numerical (DVM) and experimental (PIV) POD modes is shown in Figure 10. The first three modes are well reproduced (MAC > 0.75) and the fourth one is also reasonably well predicted (MAC = 0.47).

Figure 11 presents the energy distribution of the six POD eigenvalues. The distribution of the simulated results follows the experimental distribution. Note that the energy of the first mode from DVM results is higher than the experimental one: 87% and 78%, respectively.

The distribution of the residual energy between modes 2 to 6 is similar for the experimental results and the DVM simulations (see Figure 12). This figure also confirms the statements made in the case of the static rectangle concerning the energy level of the modes: the POD modes that are correctly identified (1 to 4) are associated with a non-negligible energy level.

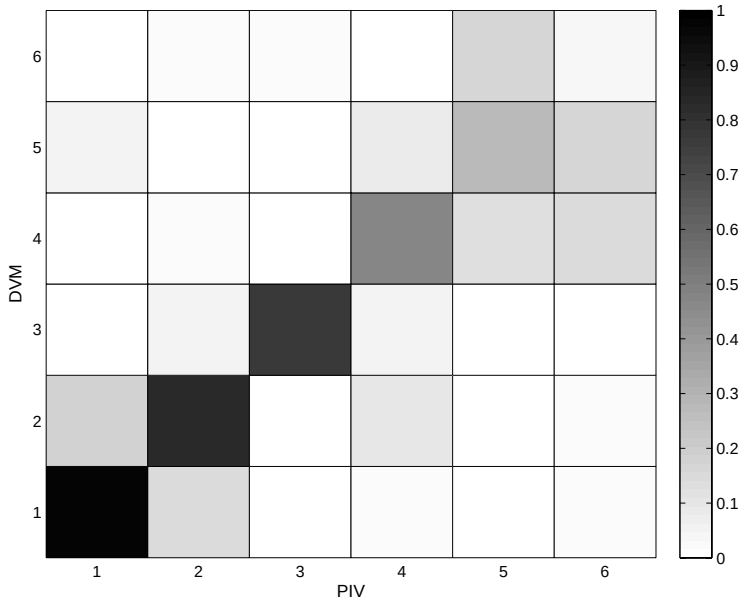


**Figure 10: Oscillating rectangle - MAC matrix of DVM vs Experiments**

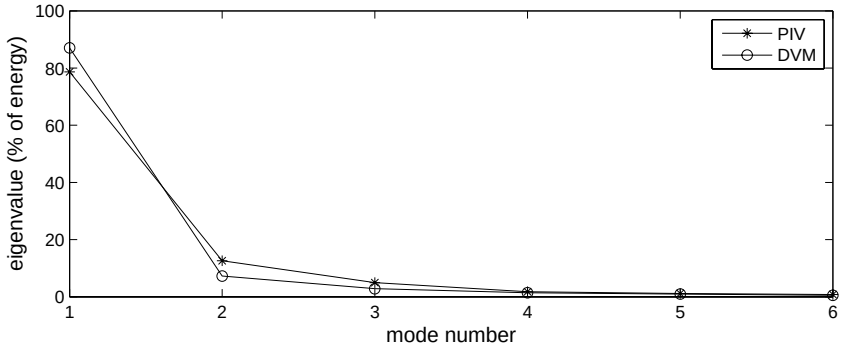


**Figure 11: Oscillating rectangle: Eigenvalues of the POD modes: percentage of the total flow energy**

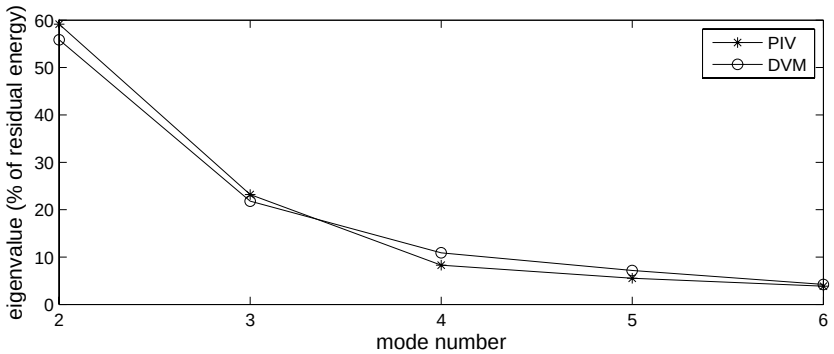


**Figure 12: Oscillating rectangle: Eigenvalues of POD modes 2 to 6: percentage of the residual flow energy**

## Discussion

Through the two applications presented in this paper, it is shown that the extraction of the first POD modes enables an effective comparison between experimental measurements and numerical results. In particular, the case of the oscillating rectangle highlights the fact that energetic simulated POD modes compare better to the experimental ones than in the static rectangular case.

The advantage of this approach is that the complete PIV measurements are used for comparing with the numerical simulations. In the case of hot wire measurements, the signal measured is better in terms of time resolution but limited in its spatial resolution. Hence, the frequency contents of the experimental and numerical data can be compared but no spatial comparison is possible. Furthermore, the use of the POD technique allows taking into account the measurements where flow separation and reattachment occur, i.e. where the flow velocities are very small and thus, very sensitive to the measurement noise. It is then an efficient method for evaluating if a numerical tool is capable of modelling flow separation and reattachment, which are of prime importance when dealing with bluff bodies.

Additionally, the MAC-matrix represents a quantitative and direct tool for comparing POD modes from experimental measurements and numerical simulations. It can be used to guide the choice of the different numerical parameters (turbulence models in the case of CFD simulations, time step or number of panels for DVM simulations, etc.). Note that the MAC and POD-based comparison method can also be used for comparing two sets of experimental data or two sets of numerical data.

Finally, a numerical tool validated in a critical region of the flow (i.e. upper surface here) by comparison of the most energetic experimental and numerical POD modes, is complementary to experimental measurements. Additional information that cannot be easily extracted from experimental fluid dynamics are then available: other quantities (pressure, vorticity,...) in other regions, with an higher resolution and in more controlled conditions. This situation is depicted in Figure 13, where the unsteady velocity field is computed over a larger domain.

In these terms, we would like to emphasize that the present POD-based validation methodology is essentially a manner of integrating CFD and experimental studies. In this way, the advantages of both approaches are combined.

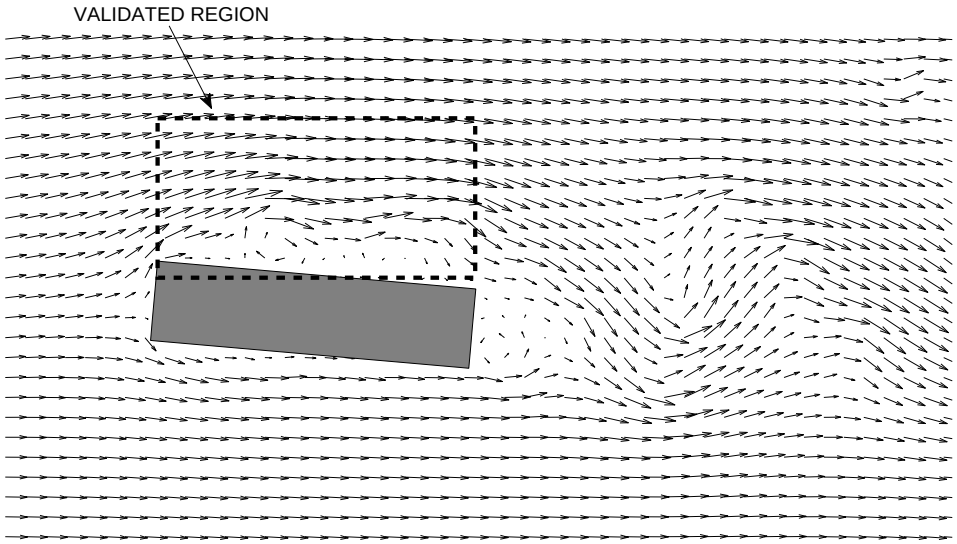


**Figure 13: Large fluid domain**

## Conclusion

This paper proposes the use of the POD technique as a preliminary step for comparing experimental measurements to numerical results. The methodology is demonstrated in the case of the flow around a bluff body, where flow separation and reattachment occur, leading to very small velocities near the surface of the body. Once extracted from the experimental measurements and the corresponding numerical simulations, the energetic patterns of the flow-field are compared.

The extraction of the most energetic characteristics of the flow-field is valuable because it simplifies the comparison between two sets of complex spatio-temporal data. The proposed method is enhanced by the use of the MAC, which results in a limited number of quantitative values.

## References

[1] P. Sagaut: *Large Eddy Simulation for Incompressible Flows*. Springer, third edition, 2006.

[2] M. Raffel, C. Willert, S. Wereley, and J. Kompenhaus: *Particle Image Velocimetry - A practical guide.* Springer, second edition, 2007.

[3] R. Mills, J. Sheridan, J. and K. Hourigan: *Particle image velocimetry and visualization of natural and forced flow around rectangular cylinders*. Journal of Fluid Mechanics, 478: 299-323, 2003.

[4] K. Mulleners and M. Raffel: *A Time-Resolved Dynamic Stall Investigation Based on Coherent Structure Analysis*. 15th International Symposium of Laser Techniques to Fluid Mechanics, Portugal, 2010.

[5] T. Andrianne, N. Abdul Razak and G. Dimitriadis: *Flow Visualization and Proper Orthogonal Decomposition of Aeroelastic Phenomena*, in Wind Tunnels, edited by Satory Okamato, ISBN 978-953-307-295-1, InTech, 2011

[6] R. Allemang and D. Brown: *A correlation coefficient for modal vector analysis*, Proccedings of the 1st International Modal Analysis Conference, p 110-116, Orlando, 1982.

[7] R. Allemang: *Vibrations: Experimental Modal Analysis*, UC-SDRL-CN-20-263-663/664, 1990.

[8] A. Léonard: *Vortex methods for flow simulation*, Journal of Computational Physics, vol. 37, pp.289-335, 1980.

[9] G. Morgenthal: *Aerodynamic analysis of structures using high-resolution vortex particle methods*, PhD Thesis, Cambridge, 2002.

[10] T. Andrianne: *Experimental and numerical investigations of the aeroelastic stability of bluff structures*, PhD Thesis, University of Liège, 2012.

[11] J.H. Ferziger and M. Peric: *Computational Method for Fluid Dynamics*. Springer, third edition, 2002.

[12] F., Menter: *Two-Equation Eddy-Viscosity Turbulence Models for Engineering Applications*, AIAA Journal, 32 (8), pp. 1598-1605, 1994.

[13] M. Casey and T. Wintergerste: *ERCOFTAC Special Interest Group on "Quality and Trust in Industrial CFD": Best Practice Guidelines*. 2000.

[14] Y. Nakamura and T. Mizota: *Torsional flutter of rectangular prisms*, Journal of the engineering mechanics division, ASCE, vol. 101, n° EM2, pp. 125-142, 1975.